Enhanced Spontaneous Light Emission of ZnO Nanowire-Based Gratings

Emmanuel Centeno, Aubry Martin, Audrey Potdevin, François Réveret, Rafik Smaali, Jesukpego Anorld Capo Chichi, Victor Kalt, Elena Kachan, Yves Jourlin, Michel Langlet, et al.

Enhanced spontaneous light emission of ZnO nanowires based gratings

Emmanuel Centeno,[*,†] Aubry Martin,[‡,¶] Audrey Potdevin,[*,¶] François Réveret,[¶] Rafik Smaali,[§] Jesukpego Anorld Capo Chichi,[§] Victor Kalt,[§] Elena Kachan,[‖] Yves Jourlin,[‖] Michel Langlet,[*,‡] and Geneviève Chadeyron[¶]

†*Université Clermont Auvergne, CNRS, Clermont Auvergne INP, Institut Pascal, F-63000 Clermont-Ferrand, France*

‡*Université Grenoble Alpes, CNRS, Grenoble INP, LMGP, 38000 Grenoble, France*

¶*Université Clermont Auvergne, CNRS, Clermont Auvergne INP, ICCF, F-63000 Clermont–Ferrand, France.*

§*Université Clermont Auvergne, CNRS, SIGMA Clermont, Institut Pascal, F-63000 Clermont-Ferrand, France*

‖*Laboratoire Hubert Curien, Université Jean-Monnet, Université de Lyon, IOGS, UMR CNRS 5516, 42000 Saint-Etienne, France*

E-mail: emmanuel.centeno@uca.fr; audrey.potdevin@sigma-clermont.fr; michel.langlet@grenoble-inp.fr

Abstract

We theoretically and experimentally investigate the spontaneous light emission of ZnO nanowires arranged in grating structures. Through systematic calculations of light extraction and absorption efficiencies together with the Purcell factor, we shed light on the influence of disorder on these optical processes. This analysis unveils the role of optical resonances to achieve directive light extraction and to enhance the spontaneous

emission. We demonstrate that the periodic structuring of the ZnO nanowires at the micron scale is a robust and efficient solution to increase the spontaneous emission efficiency.

Keywords

Spontaneous emission, Nanowires, gratings, Purcell effect, Light extraction.

Introduction

The enhancement of the spontaneous emission of emissive devices is a major issue for lighting, communication, imaging and medicine applications. The primary focus has been on increasing light-extraction efficiency (LEE) because a large amount of generated photons remain trapped due to total internal reflection within the active material. As a result, several approaches have been explored to improve the LEE including periodic structuring or random surface texturing.[1] The first solution has been implemented with dielectric photonic crystals[2,3] and gratings[4] that open diffraction orders able to extract the generated photons in selected directions. In the latter approach, the increase in light extraction stems from the scattering mechanism attributed to the intentionally roughened interface between the active material and air.[5–8] Such approaches can also benefit from the high electromagnetic confinement provided by the use of plasmonic antennas or high dielectric particles.[9–12]

Nanowire coatings represent an alternative and efficient solution to increase LEE since nanowires (NWs) behave like nano-antennas and can themselves serve as efficient emitters.[13] Zinc Oxide (ZnO) nanowires have in particular attracted much attention owing to their ease crystallization in various forms, their optoelectronic properties and their compatibility with several substrates such as GaN, Si or glass.[14] Several works have already demonstrated that ZnO arrays grown on top of LEDs improve their emission efficiency.[15–20] Moreover, various structural defects of ZnO NWs (oxygen or zinc vacancies and interstitials) give rise

to photoluminescence in different wavelength domains of the visible spectrum from 400 to 750 nm, depending on their synthesis process.[21,22] Hence, coatings made of red-emitting hydrothermally-grown ZnO NWs impregnated with YAG:Ce nanoparticles have recently demonstrated as a versatile and inexpensive promising solution to improve both emission intensity and color rendering index of white LEDs.[23]

In order to merge both periodic and random texturing approaches, the micro-structuring of ZnO NWs arranged in a one-dimensional grating[24] or in photonic crystal membranes[25] has been proposed to combine both Bragg and scattering effects. However, to our knowledge, a full study explaining the improvement of the photoluminescence quantum yield (PLQY), defined as the ratio of emitted photons to injected photons is still lacking. Indeed, its increase is not solely due to LEE but is influenced by two other mechanisms. First, electromagnetic resonances enhance the absorption of the injected photons sent by the optical pump, determining the light injection efficiency (LIE) defined as the ratio of absorbed photons to injected ones. Secondly, electromagnetic resonances occurring at the emission wavelength also boost the rate of emitted photons. This mechanism known as the Purcell effect arises when the structure acts as an open cavity where light is trapped.[26] In that case, the improvement of the PLQY is attributed to the increase in the internal quantum efficiency (IQE) - defined as the ratio of the emitted photons to the absorbed ones. This analysis leads to approximate the PLQY by the following equation:

$$PLQY = LEE \times LIE \times IQE, \tag{1}$$

In this study, we make the full calculation of the LEE, the LIE and the Purcell factor to gain a comprehensive understanding on the spontaneous emission process in ZnO nanowire-based gratings. Furthermore, we investigate how microscopic disorder influences light emission, with particular attention to its effects on the electromagnetic resonances. This work reveals the subtle role of the electromagnetic resonances in the enhancement of

the PLQY for grating structures.

Fabrication method of ZnO nanowires based structures

ZnO NW coatings and gratings have been elaborated using a two-step sol-gel / hydrothermal procedure that has been fully detailed in our previous paper and is briefly recalled hereafter.[24] A specifically developed sol-gel formulation is firstly used for the deposition by spin-coating of a ZnO-based resist thin film on 2.5 × 2.5 cm^2 quartz substrates. A crystallized ZnO film is then obtained after annealing the sample at 540°C. This film serves as a seed layer for the subsequent step. In this second step, the sample is immersed in a new ZnO-based bath heated at 90°C, which leads to the hydrothermal growth of NWs on the seed layer surface and to the formation of "full plate" NW coatings. Furthermore, the ZnO-based resist is photosensitive under UV insolation owing to the use of benzoylacetone in the sol-gel formulation. Consequently, while the resist is chemically stable before insolation, a photo-hydrolytic mechanism leads to insolated areas that are soluble in acidic media. A selective UV insolation followed by acidic washing enables therefore to photo-imprint gratings in the resist thin film. After crystallization at 540°C of the non-insolated areas, this procedure allows then the selective growth of ZnO NW gratings according to the previously described hydrothermal process. In this work, the selective insolation was performed using a quartz mask coated with chromed linear gratings of 2 µm width and 4 µm pitch. Accordingly, the amount of selectively grown NWs is expected to be twice lesser compared to a full plate NW coating. The scanning electron microscopy (SEM) image of Figure 1a shows that our experimental procedure leads to uniform and reproducible NW gratings.

The cross-section SEM image shown in Figure 1b illustrates NWs with a mean diameter around 40 nm. This cross-section image also depicts two important features that provide first insights in the disordered grating structure. On the one hand, NWs do not grow perfectly vertically, and their inclination tends to increase on the grating edges, leading to some kind

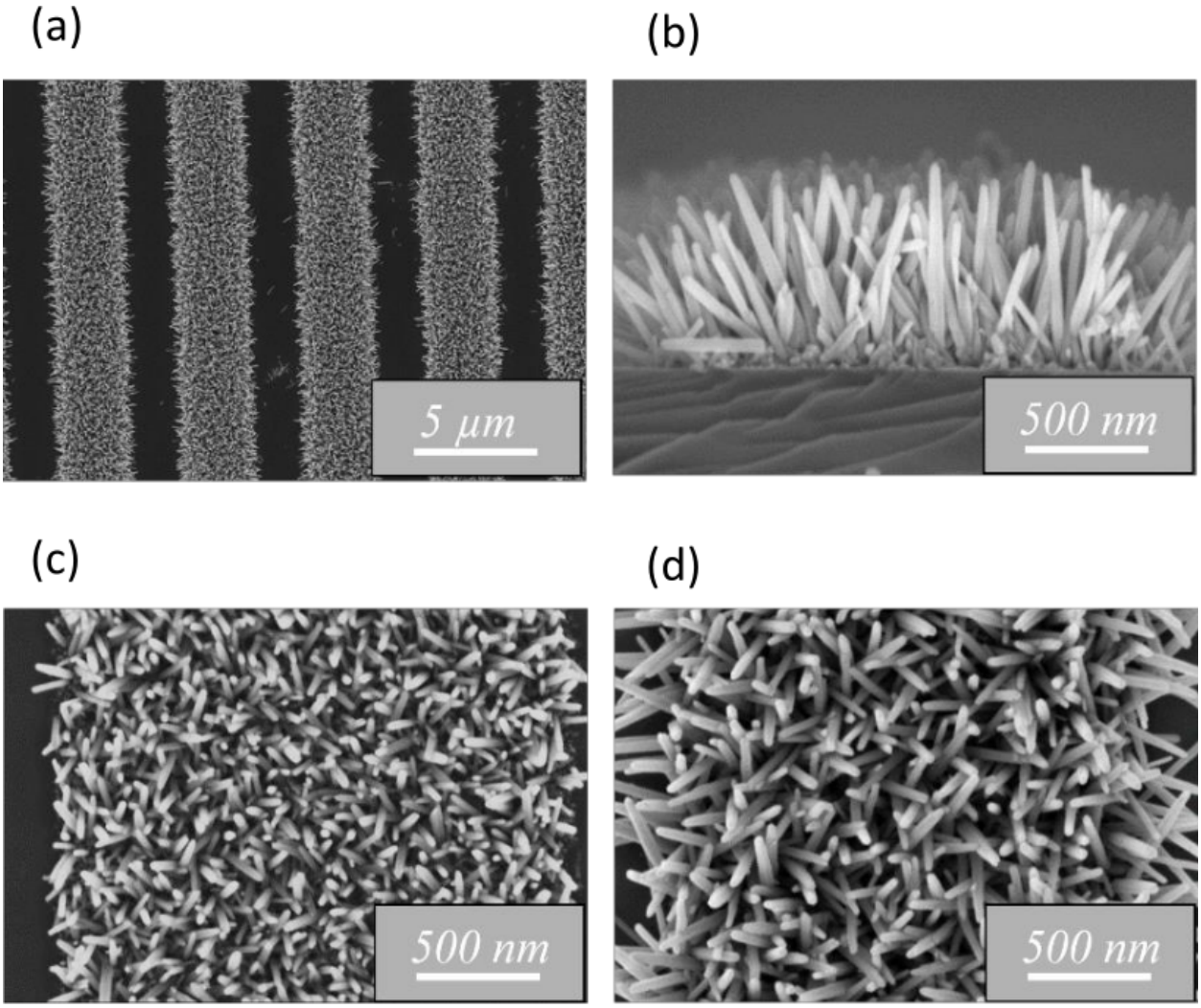

Figure 1: Low magnification top-view SEM image (a) and cross-section SEM image (b) of NW gratings obtained after a growth duration of 30 min, and high magnification top-view SEM images of a grating obtained after a growth duration of 10 (c) and 30 min (d).

of hedgehog structure whose width increases with its height. On the other hand, not all of the nanowires initially grown on the ZnO seed layer surface emerge at the grating top, inducing some local grating height variations. Both features have a direct influence on the NWs density, which exhibits thus a lateral and a vertical gradient. This is clearly depicted by top view SEM images gathered in Figures 1c and 1d. Whereas after a 10 min growth, the NWs density is quite important (Figure 1c), after a 30 min growth, it appears significantly weaker and this weakening is particularly marked on the grating edges (Figure 1d). The mean NWs density was tentatively assessed from an analysis of top view SEM images and was observed to decrease from around 280 NWs / μm^2 after a 10 min growth to around 130 NWs / μm^2 after a growth duration of 30 or 40 min. However, it is important to note that this surface density does not reliably account for the real NWs density and provides a value that is largely underestimated for thicker gratings owing to the aforementioned vertical density gradient.

The NWs grating structure has also been assessed from atomic force microscopy (AFM) measurements. As illustrated in Figure 2, the grating height is observed to reach a mean value around 200, 300, 550 and 640 nm after a growth duration of 10, 20, 30 and 40 min, respectively. The grating width is 2 µm after a 10 min growth duration (Figure 2a), which fairly corresponds to the expected value according to the chromed gratings of the used mask. Additionally, there is a gradual increase in the grating width with the growth duration (Figures 2b to 2d). This feature is related to the hedgehog grating profile whose width increases with its height. Such kind of profile can obviously not be probed by the AFM tip, which explains widths larger than the expected value when the growth duration increases. Figure 2 also depicts rough grating profiles, in agreement with local height variations illustrated in the cross-section SEM image of Figure 1b. This provides a new illustration of the disordered grating structure. For instance, for gratings of 550 nm (Figure 2c) and 640 nm mean height (Figure 2d), the roughness is observed to locally vary by around 200 nm. Electromagnetic simulations described in this paper will be more particularly focused on gratings with a typ-

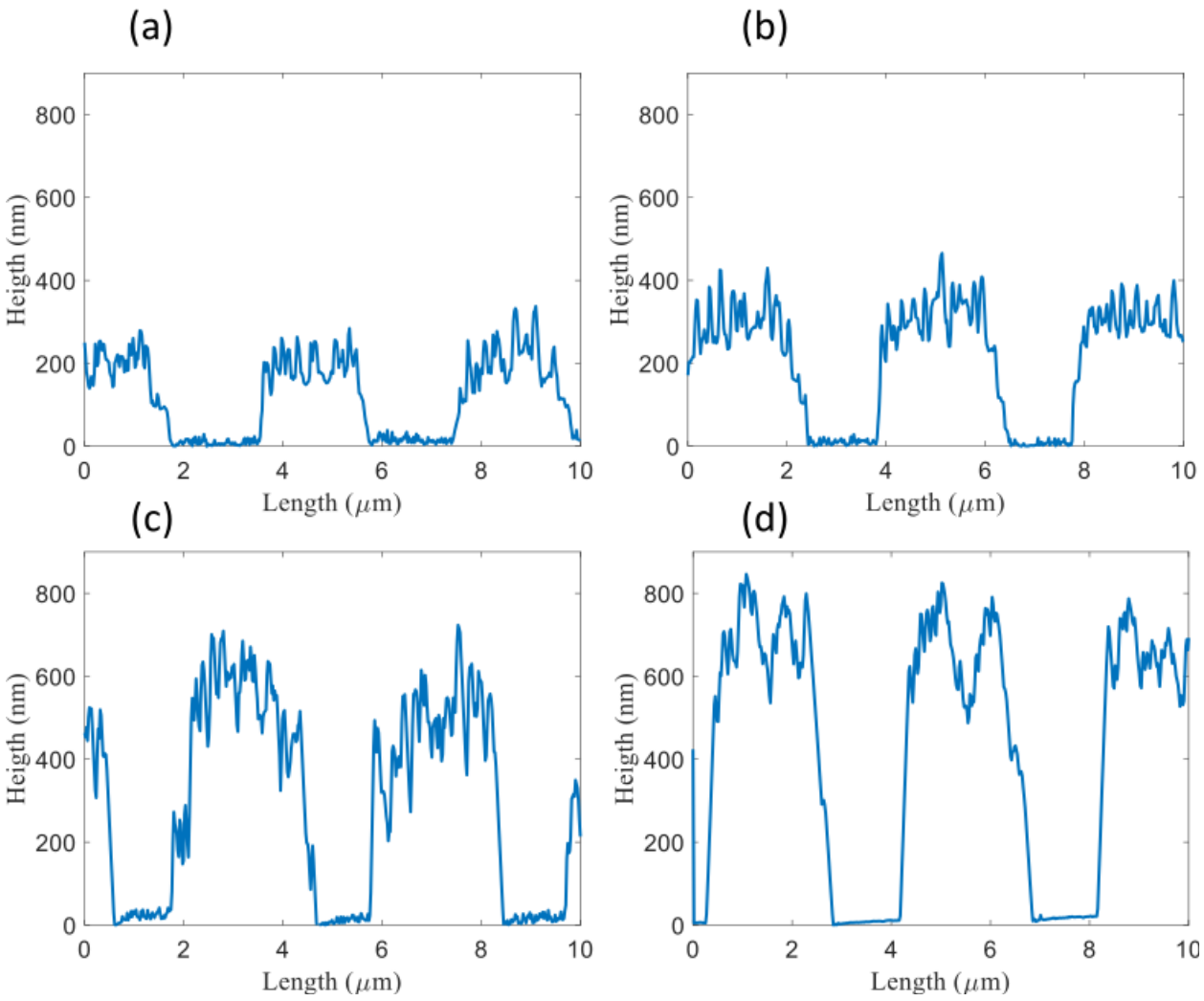

Figure 2: AFM profiles of NW gratings obtained after a growth duration of 10 (a), 20 (b), 30 (c) and 40 min (d).

ical height of 600 nm. The mean NW density was fixed at 200 NW /µm^2, which corresponds to a value averaged between the NW surface density of the thinnest and the thickest gratings studied here. Furthermore, the disordered grating structure has been taken into account in the simulations. The roughness measured by AFM would have been a valuable parameter for quantitatively describing disordered gratings. However, in the present case, such a measurement can hardly been envisaged as the AFM tip cannot properly probe the whole depth of voids separating neighbouring NWs. Besides, this measurement is all the more complicated owing to the various NW inclinations. Thus, for tentatively accounting the disordered grating structure, we have introduced a roughness Δh of 200 nm, in agreement with AFM data illustrated in Figures 2c and 2d.

Optical characterization methods

Angle resolved photoluminescence (ARPL) measurements have been performed at room temperature. A picosecond laser diode emitting at 375 nm was used to excite ZnO NW samples on the backside (quartz substrate side). The PL was detected by an optical fiber mounted on a goniometer to collect emission from 0° (in front of the top surface), to 90° (in front of the edge) with an angular resolution of 1.4°. The configuration is the same as in our previous work.[24] A 425 nm long pass filter was used to remove the excitation line. The signal was then focused on the slit of a 32 cm focal monochromator and detected by a CCD camera. The ARPL measurements for both NWs coating and grating structures are integrated across all the emission angles (from 0° to 90°).

Decay times were recorded at room temperature using a time-resolved photoluminescence (TRPL) measurement. The same excitation source as ARPL was used, with a pulse duration of 65 ps and a repetition rate of 200 kHz. The emission signal was focused on the slit of a 300 mm focal monochromator coupled with a photomultiplier. The luminescence decay is measured at an emission wavelength fixed at 600 nm. The following exponential decay

function is used to estimate the decay time: $\sum A_i e^{-t/\tau_i}$, where τ_i corresponds to the decay time and A_i to its associated weight. To find a good agreement with experimental results we take four exponential contributions in the fitting procedure. An accurate analysis of these different contributions is beyond the scope of the present manuscript, thus, to easily compare the results, we calculate an average decay time.

Theoretical and simulation tools

Models and simulation methods

This section is devoted to the presentation of the electromagnetic numerical methods developed to calculate the optical properties of the structures. The electromagnetic properties of the structures are simulated by means of the Finite Element Method (FEM) implemented in the commercial software Comsol Multiphysics.

Calculation of the dispersion properties

The intrinsic electromagnetic properties of the gratings are studied by calculating the eigenmodes supported by the structures without any incident field. Bloch boundary conditions are implemented in the periodic direction and perfectly matched layers (PML) are introduced in the transverse directions in the software Comsol Multiphysics. The calculation of the complex eigenfrequency allows to calculate the dispersion relation of the modes as a function of the transverse wavevector $k_{\|}$ and to determine the quality factor Q of the modes.

Calculation of the light extraction efficiency

Various methods, such as applying the reciprocity theorem [27,28] or directly exciting the system with discrete sources [29–31] have been used to determine the LEE. In this work, the calculation of the LEE is carried out by computing the emitted power of several dipoles randomly

distributed within the active material. This method is applied for both the ZnO NW grating and coating structures where Bloch conditions are also applied in the periodic direction as shown in Figure 3.

Here, we impose the same 4 micron period for the grating and for the coating structures. The disorder due to randomly oriented nanowires is modeled by a rough top interface between the equivalent ZnO material and air. This rough surface is described by the following equation:

$$y(x) = h_{ZnO} + \Delta h_{rand}(x) sin(\frac{2\pi}{L_{rand}} x + \phi_{rand}(x)), \tag{2}$$

where h_{ZnO} is the mean height of the homogenized ZnO layer, $\Delta h_{rand}(x)$ is a random modulation of this height and $\phi_{rand}(x)$ is a random phase which both depend on the spatial coordinate x. These functions follow a normal distribution law. We denote Δh the mean value of the perturbation height also named the roughness. The rough surface is sub-structured with a random period L_{rand} set between 100 nm and 400 nm. We also consider that each dipole presents both a random orientation and phase. The calculation of the LEE results from the average over both TE and TM polarization cases. We also average the LEE over one hundred simulations by varying the top interface according Eq. (2) and the position of the dipoles in order to replicate the randomness of the spatial distribution of the NWs and the spontaneous emission process. The averaged radiated Poynting fluxes are denoted $\Phi_{up}(\lambda, k_{\|})$ toward the air medium, $\Phi_{lat}(\lambda, k_{\|})$ in the lateral direction and $\Phi_{d}(\lambda, k_{\|})$ toward the quartz substrate. Using this method, the spectral light extraction efficiency from the structures is monitored in all emission directions by varying the Block wavevector $k_{\|}$. From these calculations, we derive the total averaged flux $\Phi_T(\lambda, k_{\|}) = \Phi_{up}(\lambda, k_{\|}) + \Phi_{lat}(\lambda, k_{\|}) + \Phi_{d}(\lambda, k_{\|})$. Considering that the ZnO nanowires exhibit a broad emission centered around 600 nm, we introduce a normalized Gaussian function that approximately reproduces the measured spectral distribution of the photoluminescence of ZnO NWs:

$$g(\lambda) = e^{-(\lambda-\lambda_0)^2/\Delta\lambda^2} \tag{3}$$

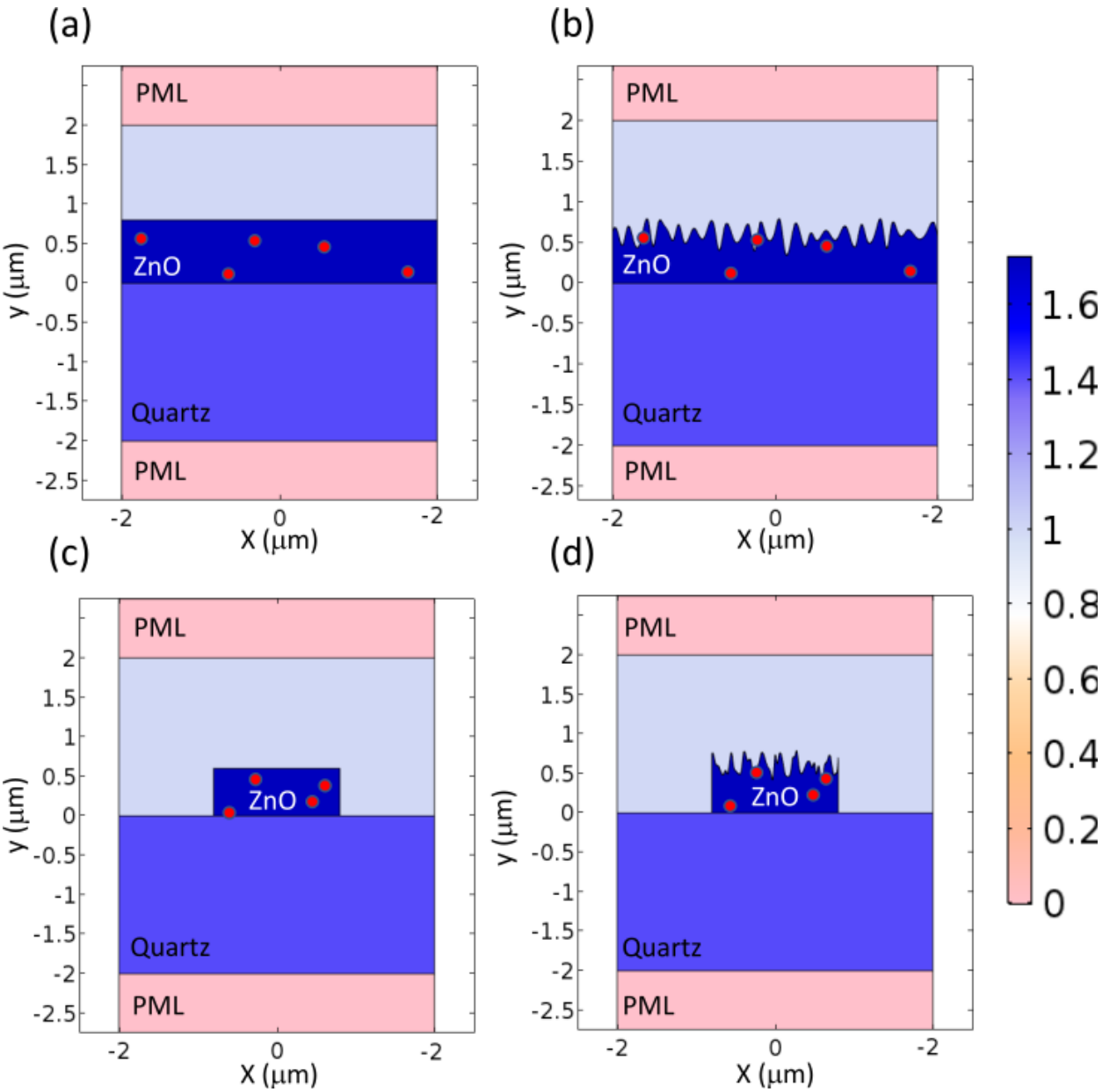

Figure 3: Schematic of the NWs based coating and grating structures. (a) and (c) correspond to the coating and grating free of disorder while (b) and (d) present a roughness. The colorbar corresponds to the refractive index of the materials. The red points are the dipoles sources randomly distributed within the active material.

where $\lambda_0 = 600$ nm and $\Delta\lambda = 100$ nm.

Lastly, the LEE toward the air medium, denoted $\eta_{up}(\lambda)$, is defined as the ratio of $\Phi_{up}(\lambda, k_\parallel)$ integrated over all emission angles (equivalently by varying the Bloch wavevector in the first Brillouin zone) to the integrated total averaged flux. This ratio is then weighted by the Gaussian intensity function:

$$\eta_{up}(\lambda) = g(\lambda)\frac{\int_{BZ}\Phi_{up}(\lambda, k_\parallel)\,dk_\parallel}{\int_{BZ}\Phi_T(\lambda, k_\parallel)\,dk_\parallel} \tag{4}$$

This approach allows us to determine the spectral distribution of the LEE for the coating and grating structures made of ZnO NWs. To comprehensively grasp the full range of extraction mechanisms, we also calculate the lateral LEE denoted $\eta_{lat}(\lambda)$ and the LEE toward the quartz substrate, $\eta_d(\lambda)$. For that, we follow the same procedure, substituting $\Phi_{up}(\lambda, k_\parallel)$ by $\Phi_{lat}(\lambda, k_\parallel)$ and $\Phi_d(\lambda, k_\parallel)$ in Eq. (4).

Results and discussion

Electromagnetic modes of nanowires coating and grating

Coatings and gratings based on ZnO NWs patterned at the micro scale form very complex electromagnetic systems that require heavy computational resources. To tackle this challenge, we initially substitute the randomly arranged ZnO array by a homogeneous material. The Maxwell-Garnet formula allows us to estimate the equivalent refractive index:

$$n_h = \sqrt{f n_{ZnO}^2 + (f-1)n_0^2}, \tag{5}$$

where f is the filling factor in NWs, $n_{ZnO} = 2$ the optical index of bulk ZnO at 600 nm and $n_0 = 1$ the air refractive index. For NWs with a diameter of 40 nm and a density of approximately 200 NW/μm^2, which are the features determined by the morphological study, the resulting equivalent optical index n_h is approximately 1.65. A similar value was

obtained from the analysis of the scanning electron microscope images of similar coatings.[32] This homogenized model enables us to assimilate the ZnO coating to a waveguide on top of a quartz substrate and the periodic pattern of the ZnO NWs to a grating made of ribbons of width W_{ZnO} and period D as depicted in Figure 4. Consequently, the ZnO coating exhibits a refractive index higher than that of the quartz substrate ($n_Q = 1.45$). We also assume a ribbon's width of 1.6 μm instead of 2 μm used for the experimental samples. This effective width is explained by the lateral decrease in the ZnO NWs density which reduces the amount of material.[24]

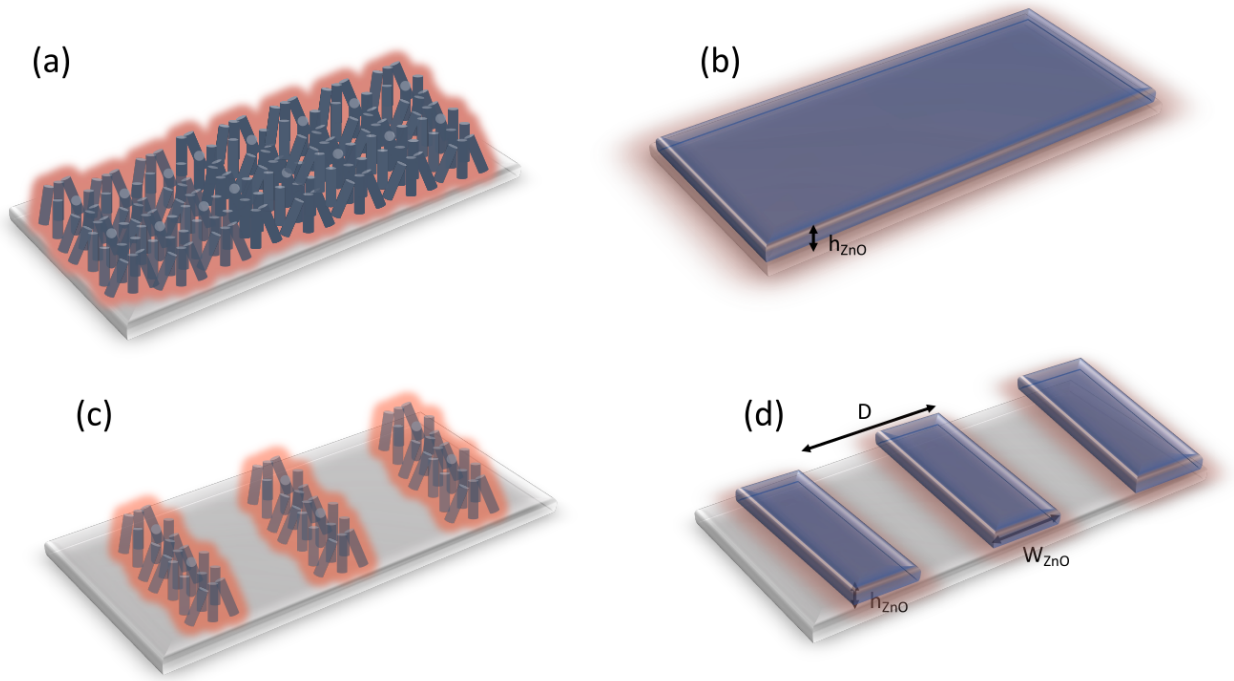

Figure 4: Schematic of the NWs based coating (a) and grating (c) and their respective homogenized counterparts: waveguide (b) and ribbon structure (d).

With this model, the presence of disorder due to the complex arrangement of the NWs is ignored. However, it provides a first insight into the optical properties of the coating and grating structures. For the waveguide structure of Figure 4b, a significant amount of the light emitted by the ZnO NWs is therefore guided within the coating by electromagnetic modes whose dispersion relations are analytically calculated. The dispersion relations indicate that the fundamental modes cannot propagate when the ratio of the waveguide height to the

wavelength, d/λ, is equal to 0.2 for TE polarization and 0.27 for TM polarization (see Figure S.1a). For example, as the coating thickness decreases to 120 nm for TE polarization and 162 nm for TM polarization, radiation emitted at wavelengths higher than 600 nm are no longer trapped in the active material.

Next, we computed the dispersion relation of resonant modes for the grating of Figure 4c presenting a period of 4 µm and composed of ribbons that are 1.6 µm wide. Figure 5 illustrates the dispersion relations of TE-polarized eigenmodes along with their corresponding quality factors Q as the ribbon height decreases from 600 nm to 200 nm. We identified two types of eigenmodes resembling the waveguide's fundamental and asymmetric modes. This observation can be intuitively understood by recognizing that the grating is made up of a periodic array of finite-length waveguides. Remark that we exclusively present the dispersion relations of the fundamental mode since the calculations show that the Q factor of the asymmetric eigenmode is smaller than 10. These dispersion relations for the grating show two important features when the thickness of the ribbon decreases to 200 nm (Figure 5c). First, the fundamental resonant mode disappears for wavelengths larger than 650 nm. Secondly, the quality factor of this mode is drastically decreased by a factor 2 compared with Figure 5a. This behavior agrees with the mode analysis for the waveguide which indicates the presence of a cut-off for the fundamental mode. Reducing the height of the ribbons below this cut-off prevents the guided mode to propagate and consequently to resonate within the finite-length waveguides. Comparable outcomes can be anticipated for the TM polarization scenario, given the similarity between the effective indices of the fundamental mode calculated for the two polarizations (as depicted in Figure S.1a).

We have shown in reference[24] that the theoretical dispersion relation corresponding to a ribbon height of 600 nm (Figure 5a) agrees with the experimental relationship deduced from ARPL measurements. This result suggests that the PL of the grating is boosted by the fundamental guided mode resonating within finite-length waveguides. To validate this hypothesis, we carried out ARPL measurements for gratings of decreasing heights. The

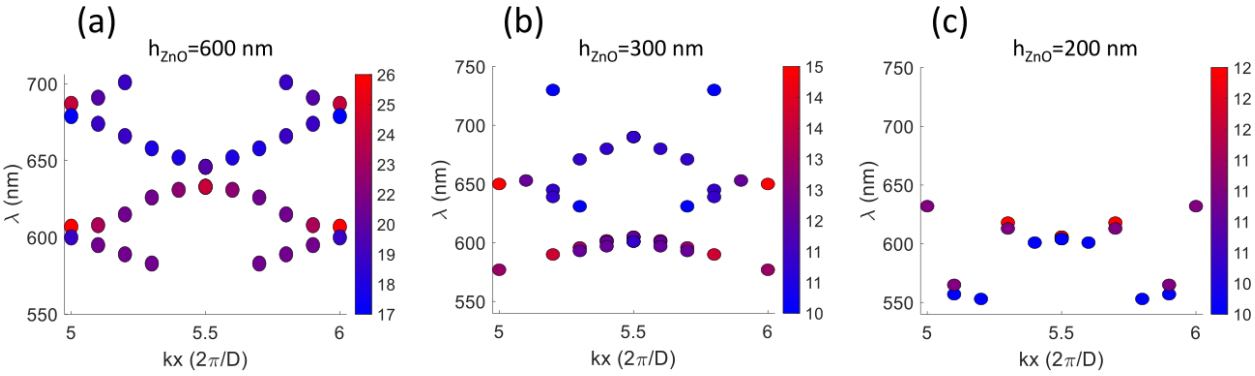

Figure 5: Dispersion relations of TE-polarized resonant modes for gratings made of ribbons of refractive index $n_h = 1.65{,}1.65\ \mu m$ wide and for three ribbon heights: (a) $h_{ZnO} = 600$ nm and (b) $h_{ZnO} = 300$ nm (c) $h_{ZnO} = 200$ nm. The color bar indicates the value of the Q factor.

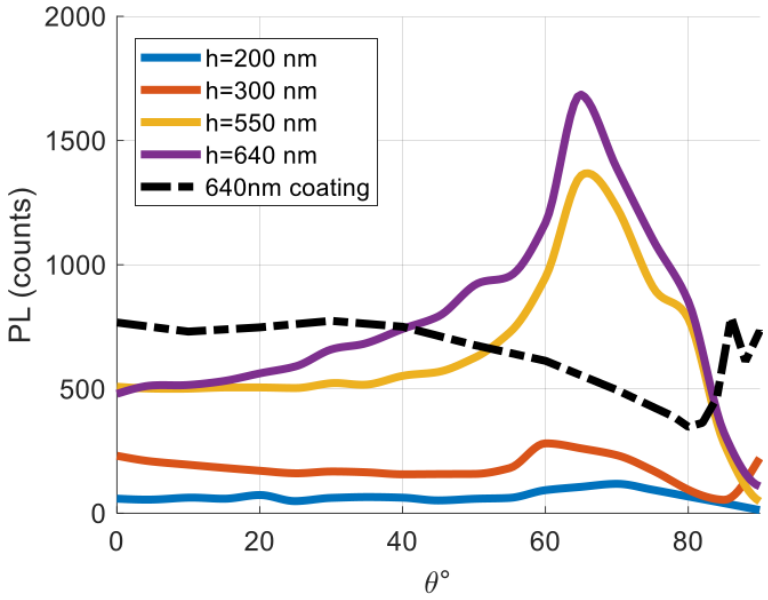

Figure 6: ARPL measurements for an emission wavelength of 600 nm for gratings of 4 μm periods, 2 μm strips width, recorded for different grating heights at room temperature. The dashed curve corresponds to the ARPL measurements for a 640 nm coating. The excitation wavelength is 375 nm.

ARPL spectra measured at the emission wavelength of 600 nm show emission peaks at 65° and 66° for gratings with respective heights of 640 nm and 550 nm, see Figure 6. These resonances reveal that the fundamental guided mode is phase-matched with the emitted plane wave corresponding to the fifth diffraction order of the grating.[24] In comparison, a 640 nm-thick NWs coating presents an almost constant PL from 0° to 40° indicating a diffuse emission due to the scattering extraction process. However, the resonant emission around 65° for the grating nearly disappears for thinner gratings, 200 nm and 300 nm high. In agreement with the theoretical mode analysis, as the wavelength approaches the cut-off of the waveguide, the fundamental mode is less and less confined within the NW gratings leading to a degradation of the resonance. These results indicate that, to improve PL, the resonance of the fundamental mode must be increased by carefully choosing the appropriate parameters for the gratings.

Impact of the disorder on the light extraction efficiency

We calculate the LEE of both waveguide and ribbon structures depicted in Figure 4b and Figure 4d, in the absence of roughness ($\Delta h = 0$), using simulations based on the calculation of the Poynting flux emitted by random dipoles. In this analysis, we assume that the waveguide and the ribbons present the same thickness equal to 600 nm.

These calculations demonstrate that the ribbon structure exhibits a significant LEE towards the air, reaching up to 61% at the nominal wavelength of 600 nm (η_{up} in Figure S.2a) indicating that this structure adeptly redirects the emitted light towards the air, thereby demonstrating its efficiency. Conversely, the waveguide presents a LEE towards air about 20% (η_{up} in Figure S.2b). In that case, the lateral LEE attains almost 75% (η_{lat} in Figure S.2b) at the nominal wavelength, strongly highlighting the phenomenon of total internal reflection. Subsequently, we simulate the presence of the disordered nanowires by introducing a rough interface with a roughness Δh equal to 200 nm in accordance with AFM measurements of the grating profile (Figure 2). In the case of the grating, the light extraction

efficiencies remain almost unaffected by the presence of the roughness for the ribbons and reach a value of 63 % at the nominal wavelength as depicted in Figure 7a. Conversely, for rough coating, which emulates a coating made of NWs, the LEE towards the surrounding air (η_{up}) demonstrates a substantial increase, reaching 61%, Figure 7a. We also observe that a weaker roughness of 100 nm already increases η_{up} for the waveguide. This outcome confirms that ZnO nanowires do indeed function as efficient scatterers, facilitating the extraction of light emission.

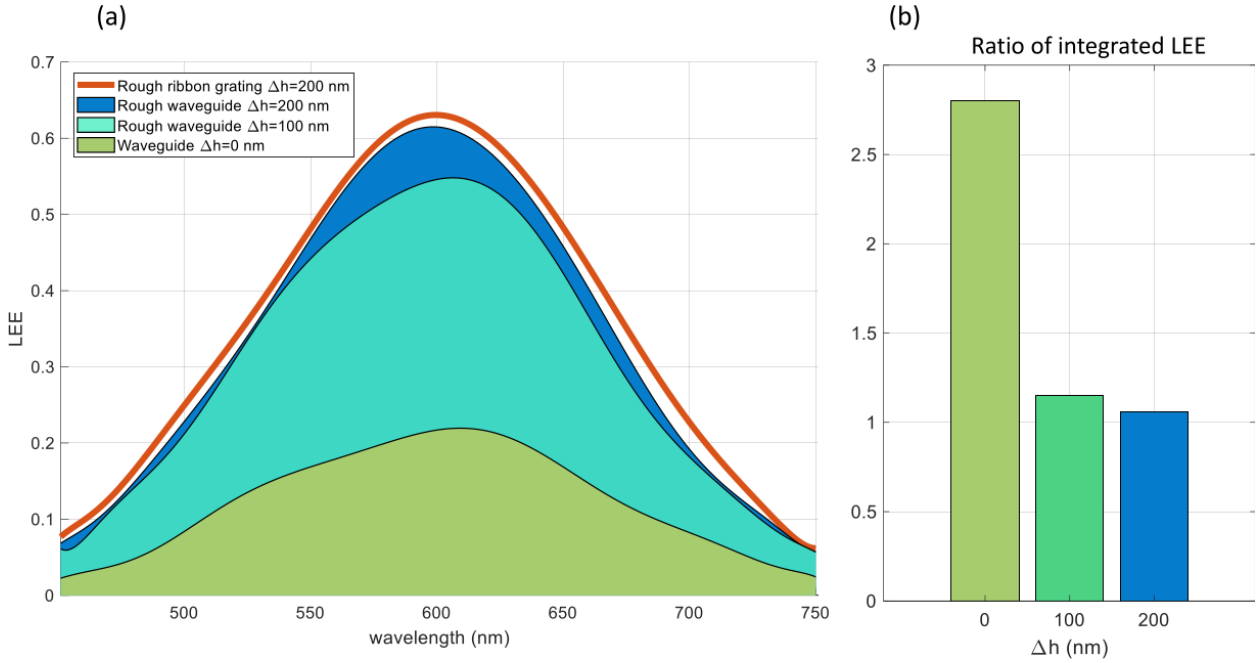

Figure 7: (a) Comparison of the light extraction efficiency toward air (η_{up}) for the waveguide and the ribbon grating and for different roughness Δh. (b) Ratios of the integrated LEE for the rough ribbon grating with $\Delta h = 200$ nm to that of the waveguide as a function of the roughness.

To quantitatively compare these light extraction efficiencies, we integrate LEE across the entire emission spectrum: $\eta_{up} = \int \eta_{up}(\lambda) d\lambda$. Next, we represent on Figure 7b the ratio, denoted R_{LEE}, of the integrated LEE for the rough ribbon grating (which presents the highest LEE) to that of the rough waveguides. These calculations demonstrate that the LEE of the rough ribbon grating exceeds that of the waveguide free of roughness by a factor of 2.8. However, when roughness is introduced for the waveguide, R_{LEE} decreases to 1.15 and

to 1.06 for perturbation Δh of 100 nm and 200 nm respectively. A similar result is observed at an emission wavelength of 600 nm, with a R_{LEE} of 1.02 for a perturbation of 200 nm, demonstrating that the grating and coating structures are equally effective at extracting the emitted photons. The main difference lies in the grating's ability to emit light at a specific angle of 64°, in contrast to the broader angular distribution observed with the coating, as shown by the ARPL measurements in Figure 6.

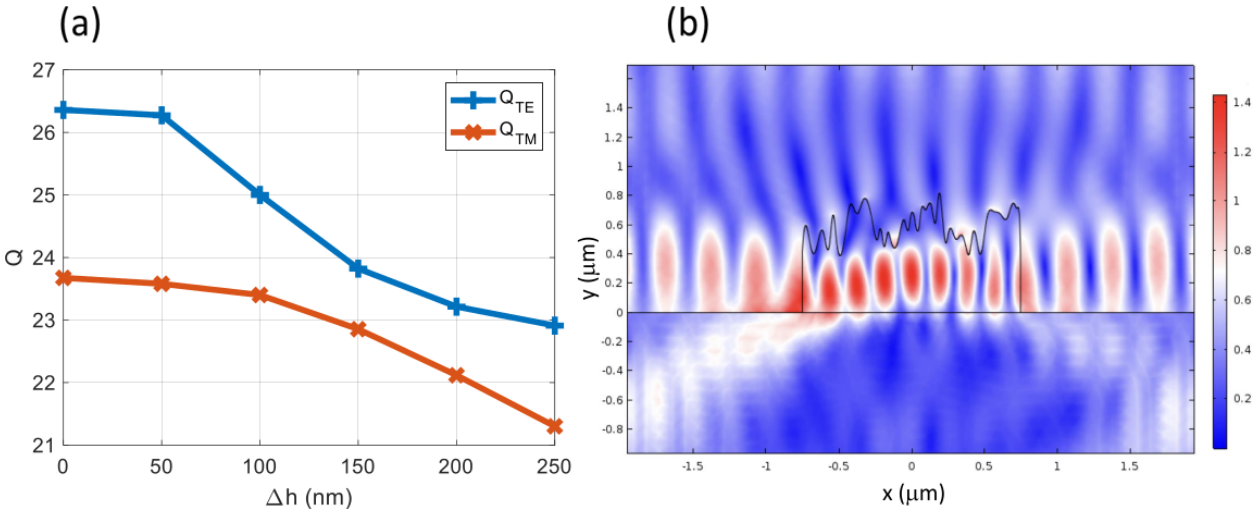

Figure 8: (a) Quality factor of the resonant mode calculated around the 600 nm wavelength for both TE and TM polarizations as a function of the perturbation height. (b) Modulus of the electric field (in TE polarization) at 600 nm for $\Delta h = 200$ nm.

This study sheds light on the robustness of the LEE of the grating in presence of roughness. Indeed, one might expect disorder to degrade the resonators formed by the periodic ribbon array. To investigate this phenomenon, the quality factor of the resonant mode is determined at a wavelength of 600 nm, while considering varying levels of perturbation height. Once again, the results are averaged over 100 simulations, involving the calculation of eigenmodes for ribbons with random profiles. As shown in Figure 8a, marginal decreases of 12 % and 6 % in the Q factor are instead observed for the TE and TM polarizations respectively. This outcome underlines the robustness of the ribbons in the face of structural disorder, as evidenced by their ability to maintain the resonant mode, as depicted in Figure 8b.

Light injection efficiency for the grating

Reducing the number of NWs by half in the grating, in comparison to the coating, results in a decreased absorption of photons within the active medium. Consequently, there is a decrease in the conversion of injected ultraviolet photons into emitted visible photons. This photoluminescence conversion mechanism relies on the absorbed power $\iiint_V \mathbf{j}\mathbf{E}dV$, which is defined by the product of the current density $\mathbf{j}$ and the electric field $\mathbf{E}$ integrated over the volume V of the active material.

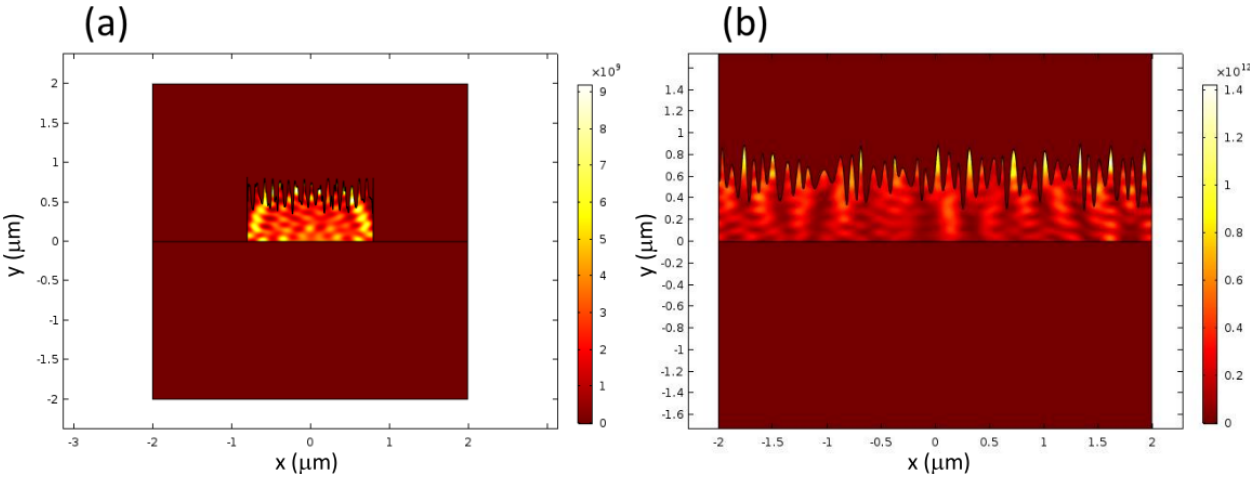

Figure 9: Maps of the density absorbed power (in W.m^{-3} and for TE polarization) computed for a plane wave in normal incidence and for a 375 nm wavelength: (a) for the grating, (b) for the coating.

To compare the LIE of the grating and that of the coating, we calculated the power absorbed when a plane wave with a wavelength of 375 nm illuminates these structures in normal incidence. At this wavelength, ZnO NWs exhibit a refractive index of 1.7 and an absorption coefficient of 0.04, as reported in reference.[33] These computations were averaged over 100 simulations to account for structural disorder and over the TE and TM polarizations. As the incident pump power remains constant for both structures, the ratio of their LIE is equal to the ratio of their corresponding absorbed powers. These calculations demonstrate that the ratio of the LIE of the grating to that of the coating, denoted R_{LIE}, is equal to 0.58 instead of the anticipated 0.5 value. This counter-intuitive result is attributed to the

additional resonances occurring in the grating at ultraviolet frequency, which increase the absorption of injected photons, as illustrated in Figure 9.

Purcell factor for the grating

The final parameter that needs to be calculated relates to the internal quantum efficiency (IQE). Since the grating can be assimilated to a periodic set of cavities, we can anticipate an increase in the number of emitted photons due to the Purcell effect. To perform the calculation of the Purcell factor, denoted $F(\lambda)$, we place a dipole at the middle of a unique ribbon, and we divide the total power radiated by a dipole, P_r, by the total power radiated in vacuum, P_{vac} :

$$F(\lambda) = \frac{P_r}{P_{vac}} \tag{6}$$

This calculation is averaged over the horizontal and vertical orientations of the dipole.

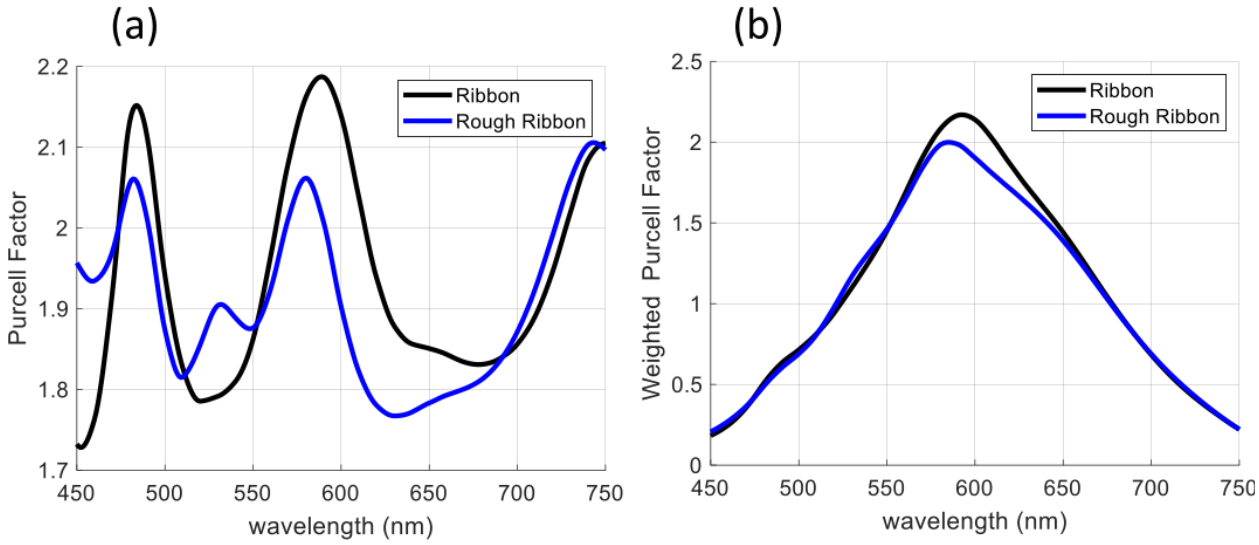

Figure 10: (a) Purcell factor, $F(\lambda)$, calculated for a ribbon and a rough ribbon of 600 nm height with a perturbation height Δh=200 nm. (b) Purcell factor weighted by the PL spectrum of the NWs, $g(\lambda) \times F(\lambda)$, with the same parameters.

The simulations reveal that the Purcell factor exceeds 2 at three specific wavelengths, 480 nm, 590 nm, and 750 nm, for a grating of 600 nm height, as shown in Figure 10 a. These wavelengths correspond to the high Q factor, which is attained at the edges of the Brillouin

zone as depicted in Figure 5a. These electromagnetic resonances for a unique ribbon have indeed been demonstrated to originate from Fabry-Perot interference.[24] The Purcell factor slightly decreases when roughness of Δh=200 nm is introduced at the upper interface of the ribbon. To determine the Purcell effect of the ZnO NWs forming the cavity, we calculate the Purcell factor weighted by PL spectrum : $g(\lambda) \times F(\lambda)$. The results presented in Figure 10b indicate that even in the presence of disorder, the ribbon retains a Purcell factor up to 2 at a wavelength of 590 nm. This outcome underlines the fact that the resonant behavior of the ribbon enhances the internal quantum efficiency of the ZnO nanowires. We conclude that at the emission peak (for λ =600 nm) the ratio of the IQE for the grating to the coating is R_{IQE}=2.

Light efficiencies balance

Gratings based on ZnO NWs patterned at the micron scale reveal very interesting properties for enhancing spontaneous light emission. As shown lastly, IQE is increased by a factor R_{IQE}=2 thanks to the Purcell effect, since the ribbons function as open cavities. Notably, the resonant behavior of the grating not only enhances the spontaneous emission rate of the NWs but also increases the absorption of injected UV photons. Despite the grating present an half of amount of NWs, its absorption efficiency only decreases by a ratio R_{LIE}=0.58. Our simulations have shown that the electromagnetic resonances remain robust in the presence of roughness, making the grating just as effective as the coating in extracting light for a roughness Δh = 200 nm. This outcome results in a ratio of LEE close to one: R_{LEE}=1. Finally, from Eq. (1), the ratio of the PLQY for the grating to that of the coating is thus given by:

$$R_{PLQY} = R_{LIE} \times R_{LEE} \times R_{IQE} \tag{7}$$

The theoretical value obtained from the calculation of the ratios of the LIE, LEE and IQE gives R_{PLQY} = 1.16 at the emission wavelength of 600 nm. The periodic structuring of the

ZnO NWs at the micron scale is therefore a robust and efficient solution to increase the spontaneous emission efficiency.

Optical measurements

To confirm this result, we performed TRPL decay measurements for the gratings and coatings at the emission wavelength of 600 nm, as shown in Figure 11. The fitted fluorescent lifetimes

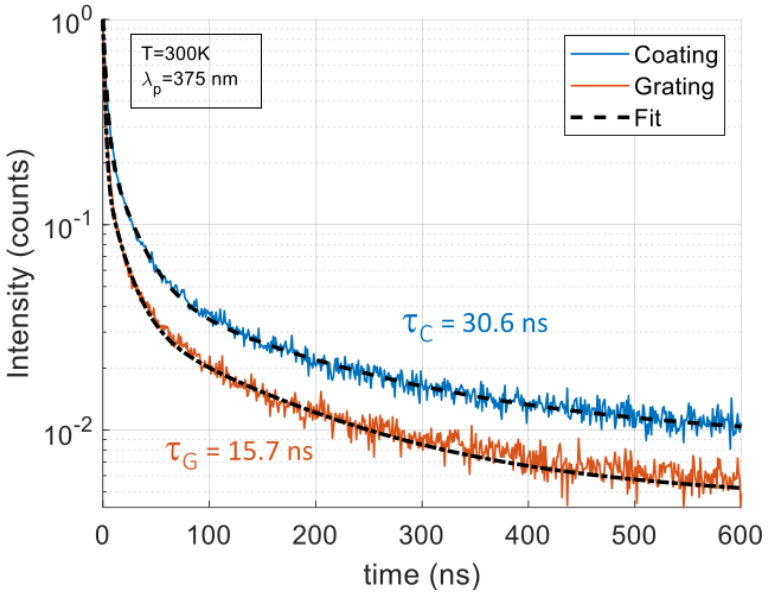

Figure 11: Comparison of the measured time-resolved photoluminescence decay for the coating and the grating of 640 nm height. The measurement are made at 300K for an excitation wavelength of $\lambda_p = 375$ nm.

for the coating and the grating are respectively $\tau_C = 30.6$ ns and $\tau_G = 15.7$ ns. Since the Purcell effect cannot occur in the coating because this structure does not support any electromagnetic resonance, the lifetime associated with the luminescence from this type of sample should be similar to that in vacuum. This assumption allows us to determine the experimental Purcell factor, which is given by $F_{exp} = \tau_C/\tau_G$, resulting in a value of 1.95. This value is in full agreement with the theoretical result and highlights that the internal quantum efficiency of the ZnO NWs arranged in a grating structure is twice as high as that of the coating.

Finally, we present the experimental PL spectra for both the coating and grating structures in Figure 12. These curves are derived from integrating the ARPL data over the whole range of emission angles. To experimental ratio of the PLQY for these structures, calculated at the 600 nm emission peak, is $R^{exp}_{PLQY} = 1.08$. This demonstrate that the efficiency of the grating slightly exceeds that of the coating.

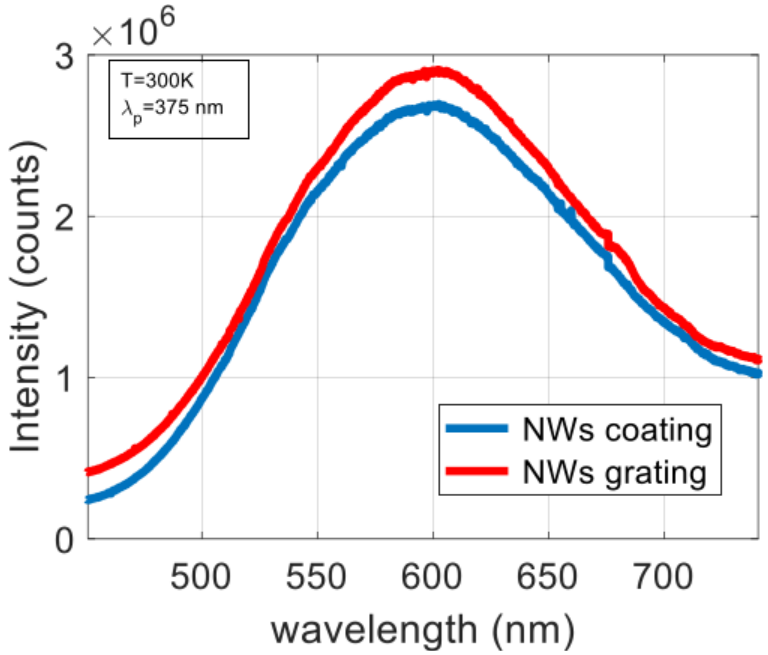

Figure 12: Emission intensity of the PL for the coating and the grating made of ZnO NWs measured at 300K for an excitation wavelength of 375 nm.

The excellent agreement between the theoretical ratio, $R_{PLQY} = 1.16$, and the experimental one, $R^{exp}_{PLQY} = 1.08$, confirms that the periodic structuring of the ZnO NWs is beneficial for the increase in the spontaneous emission.

Conclusion

In conclusion, this work explores the intricate world of electromagnetic modes within ZnO nanowire coatings and gratings, shedding light on their behavior and potential applications. We first demonstrated that the bands of the grating act like finite-length waveguides, exhibiting electromagnetic resonances. Both theoretical and experimental studies have shown that

the grating height plays a crucial role. Below a critical thickness determined by the waveguide cut-off frequency, resonance cannot build up, resulting in photoluminescence breakdown. Furthermore, the article emphasizes the impact of disorder on light extraction efficiency. Our theoretical analysis reveals that periodic structuring competes favorably with the scattering approach used in the coating, even in the presence of roughness within the ribbons. Additionally, our calculations demonstrate the resilience of grating structures in the face of disorder, without significant degradation of the ribbon quality factor. This behavior is vital to maintain high photon absorption and enhance the emission rate through the Purcell effect.

Both theoretical and experimental results confirm that gratings made of ZnO nanowires exhibit a twofold increase in the emission rate, compensating for the halving of the amount of active material. The structuring of ZnO nanowires opens up promising opportunities to manipulate the fundamental processes that enhance spontaneous emission, which is a critical advancement for applications in photonics and optoelectronics.

Acknowledgement

The authors thank the French “Agence Nationale de la Recherche” for its financial support in the frame of the ANR SMARtLEDs project (ANR-19CE08-0001).

Associated content

Supporting Information available: ”Electromagnetic study of guided modes for ZnO NWs coatings”, ”Dispersion relation diagram”, ”Light extraction efficiencies for the grating and the coating structure”.

References

(1) Zhmakin, A. I. Enhancement of light extraction from light emitting diodes. *Physics Reports* **2011**, *498*, 189–241.

(2) McGroddy, K.; David, A.; Matioli, E.; Iza, M.; Nakamura, S.; DenBaars, S.; Speck, J.; Weisbuch, C.; Hu, E. Directional emission control and increased light extraction in GaN photonic crystal light emitting diodes. *Applied physics letters* **2008**, *93*, 103502.

(3) Do, Y. R.; Kim, Y. C.; Song, Y.-W.; Cho, C.-O.; Jeon, H.; Lee, Y.-J.; Kim, S.-H.; Lee, Y.-H. Enhanced light extraction from organic light-emitting Diodes with 2D SiO2/SiNx photonic crystals. *Advanced Materials* **2003**, *15*, 1214–1218.

(4) Ziebarth, J. M.; Saafir, A. K.; Fan, S.; McGehee, M. D. Extracting Light from Polymer Light-Emitting Diodes Using Stamped Bragg Gratings. *Advanced Functional Materials* **2004**, *14*, 451–456.

(5) Wei, T.; Kong, Q.; Wang, J.; Li, J.; Zeng, Y.; Wang, G.; Li, J.; Liao, Y.; Yi, F. Improving light extraction of InGaN-based light emitting diodes with a roughened p-GaN surface using CsCl nano-islands. *Optics Express* **2011**, *19*, 1065–1071.

(6) Zhang, Y.; Li, J.; Wei, T.; Liu, J.; Yi, X.; Wang, G.; Yi, F. Enhancement in the light output power of GaN-based light-emitting diodes with nanotextured indium tin oxide layer using self-assembled cesium chloride nanospheres. *Japanese Journal of Applied Physics* **2012**, *51*, 020204.

(7) Hong, S.-H.; Kim, J.-J.; Kang, J.-W.; Jung, Y.-S.; Kim, D.-Y.; Yim, S.-Y.; Park, S.-J. Enhanced optical output of InGaN/GaN near-ultraviolet light-emitting diodes by localized surface plasmon of colloidal silver nanoparticles. *Nanotechnology* **2015**, *26*, 385204.

(8) Khaywah, M.; Potdevin, A.; Réveret, F.; Mahiou, R.; Ouerdane, Y.; Désert, A.; Parola, S.; Chadeyron, G.; Centeno, E.; Smaali, R.; Moreau, A. Large and Versatile Plasmonic Enhancement of Photoluminescence Using Colloidal Metallic Nanocubes. *The Journal of Physical Chemistry C* **2021**, *125*, 7780–7790.

(9) Lozano, G.; Louwers, D. J.; Rodríguez, S. R.; Murai, S.; Jansen, O. T.; Verschuuren, M. A.; Gómez Rivas, J. Plasmonics for solid-state lighting: enhanced excitation and directional emission of highly efficient light sources. *Light: Science & Applications* **2013**, *2*, e66–e66.

(10) Sugimoto, H.; Yashima, S.; Fujii, M. Hybridized plasmonic gap mode of gold nanorod on mirror nanoantenna for spectrally tailored fluorescence enhancement. *Acs Photonics* **2018**, *5*, 3421–3427.

(11) Staude, I.; Pertsch, T.; Kivshar, Y. S. All-dielectric resonant meta-optics lightens up. *Acs Photonics* **2019**, *6*, 802–814.

(12) Alhalaby, H.; Zaraket, H.; Principe, M. Enhanced photoluminescence with dielectric nanostructures: A review. *Results in Optics* **2021**, *3*, 100073.

(13) Leung, S.-F.; Zhang, Q.; Xiu, F.; Yu, D.; Ho, J. C.; Li, D.; Fan, Z. Light management with nanostructures for optoelectronic devices. *The journal of physical chemistry letters* **2014**, *5*, 1479–1495.

(14) Witkowski, B. Applications of ZnO Nanorods and Nanowires–A Review. *Acta Physica Polonica, A.* **2018**, *134*.

(15) Soh, C.; Tay, C.; Chua, S.; Le, H.; Ang, N.; Teng, J. Optimization of hydrothermal growth ZnO nanorods for enhancement of light extraction from GaN blue LEDs. *Journal of crystal growth* **2010**, *312*, 1848–1854.

(16) Park, Y. J.; Song, H.; Ko, K. B.; Ryu, B. D.; Cuong, T. V.; Hong, C.-H. Nanostructural effect of ZnO on light extraction efficiency of near-ultraviolet light-emitting diodes. *Journal of Nanomaterials* **2016**, *2016*.

(17) Jeong, H.; Salas-Montiel, R.; Lerondel, G.; Jeong, M. S. Ultraviolet, blue, and green InGaN-based light-emitting diodes functionalized with ZnO nanorods. *Journal of Alloys and Compounds* **2017**, *708*, 612–618.

(18) Huang, L.; Zhang, F.; Yuan, D.; Liu, B.; Cheng, C. Enhanced light output of scintillators by ZnO nanorod arrays. *Physica E: Low-dimensional Systems and Nanostructures* **2022**, *142*, 115326.

(19) Zhong, J.; Chen, H.; Saraf, G.; Lu, Y.; Choi, C.; Song, J.; Mackie, D.; Shen, H. Integrated ZnO nanotips on GaN light emitting diodes for enhanced emission efficiency. *Applied Physics Letters* **2007**, *90*, 203515.

(20) Jeong, H.; Park, D. J.; Lee, H. S.; Ko, Y. H.; Yu, J. S.; Choi, S.-B.; Lee, D.-S.; Suh, E.-K.; Jeong, M. S. Light-extraction enhancement of a GaN-based LED covered with ZnO nanorod arrays. *Nanoscale* **2014**, *6*, 4371–4378.

(21) Vempati, S.; Mitra, J.; Dawson, P. One-step synthesis of ZnO nanosheets: a blue-white fluorophore. *Nanoscale research letters* **2012**, *7*, 1–10.

(22) Zhang, Y.; Apostoluk, A.; Theron, C.; Cornier, T.; Canut, B.; Daniele, S.; Masenelli, B. Doping of ZnO inorganic-organic nanohybrids with metal elements. *Scientific Reports* **2019**, *9*, 11959.

(23) Amara, N.; Martin, A.; Potdevin, A.; Riassetto, D.; Messaoud, M.; Réveret, F.; Chadeyron, G.; Bouaziz, J.; Langlet, M. ZnO nanowires/YAG: Ce functional heterostructure coatings with tunable optical properties. *Journal of Alloys and Compounds* **2020**, *842*, 155708.

(24) Martin, A.; Potdevin, A.; Réveret, F.; Centeno, E.; Smaali, R.; Omeis, F.; Riassetto, D.; Kachan, E.; Jourlin, Y.; Chadeyron, G.; Langlet, M. Study of the Photoluminescence Enhancement Observed in ZnO Nanowire Gratings Optimally Grown by the Hydrothermal Method. *Advanced Optical Materials* **2023**, 2300695.

(25) Yin, Z.; Liu, X.; Wang, H.; Wu, Y.; Hao, X.; Ji, Z.; Xu, X. Light transmission enhancement from hybrid ZnO micro-mesh and nanorod arrays with application to GaN-based light-emitting diodes. *Optics Express* **2013**, *21*, 28531–28542.

(26) Noda, S.; Fujita, M.; Asano, T. Spontaneous-emission control by photonic crystals and nanocavities. *Nature photonics* **2007**, *1*, 449–458.

(27) Zhang, S.; Martins, E. R.; Diyaf, A. G.; Wilson, J. I.; Turnbull, G. A.; Samuel, I. D. Calculation of the emission power distribution of microstructured OLEDs using the reciprocity theorem. *Synthetic Metals* **2015**, *205*, 127–133.

(28) Sun, S.; Zhang, T.; Liu, Q.; Ma, L.; Du, Q.; Duan, H. Enhanced directional fluorescence emission of randomly oriented emitters via a metal–dielectric hybrid nanoantenna. *The Journal of Physical Chemistry C* **2019**, *123*, 21150–21160.

(29) Lee, H. K.; Ko, Y. H.; Raju, G. S. R.; Yu, J. S. Light-extraction enhancement and directional emission control of GaN-based LEDs by self-assembled monolayer of silica spheres. *Optics Express* **2012**, *20*, 25058–25063.

(30) Kim, J.-W.; Jang, J.-H.; Oh, M.-C.; Shin, J.-W.; Cho, D.-H.; Moon, J.-H.; Lee, J.-I. FDTD analysis of the light extraction efficiency of OLEDs with a random scattering layer. *Optics express* **2014**, *22*, 498–507.

(31) Ding, P.; Shao, L.; Wang, J.; Li, Y.; Zeng, F.; Liang, E. Enhanced light extraction with silicon nanoantenna arrays for white light LED applications. *Optical and Quantum Electronics* **2017**, *49*, 1–14.

(32) Amara, N.; Martin, A.; Potdevin, A.; Réveret, F.; Riassetto, D.; Chadeyron, G.; Langlet, M. Nanostructuration of YAG: Ce Coatings by ZnO Nanowires: A Smart Way to Enhance Light Extraction Efficiency. *Nanomaterials* **2022**, *12*, 2568.

(33) Stelling, C.; Singh, C. R.; Karg, M.; König, T. A.; Thelakkat, M.; Retsch, M. Plasmonic nanomeshes: their ambivalent role as transparent electrodes in organic solar cells. *Scientific reports* **2017**, *7*, 42530.

TOC Graphic